The FuGas 2.2 framework for atmosphere-ocean coupling in geoscientific models: comparing and improving algorithms for the estimates of the solubilities and fluxes of greenhouse gases and DMS

Vasco M. N. C. S. Vieira[1], Pavel Jurus[2,5], Emanuela Clementi[3], Heidi Pettersson[4] and Marcos Mateus[1].

[1]MARETEC, Instituto Superior Técnico, Universidade de Lisboa, Av Rovisco Pais, 1049-001 Lisboa, Portugal.
[2]DataCastor, U Svobodarny 1063/6,190 00 Praha 9, Prague, Czech Republic.
[3]Istituto Nazionale di Geofisica e Vulcanologia, INGV, Bologna, Italy.
[4]Finnish Meteorological Institute, P.O. Box 503, FI-00101 Helsinki, Finland.
[5]Institute of Computer Science, Czech Academy of Sciences, Prague, Czech Republic.

Correspondence to: Vasco M. N. C. S. Vieira vasco.vieira@tecnico.ulisboa.pt

ABSTRACT

Accurate estimates of the atmosphere-ocean balances and fluxes of greenhouse gases and DMS are fundamental for geoscientific models dealing with climate change. A significant part of these fluxes occur at the coastal ocean which, although much smaller than the open ocean, is also much more heterogenic. The scientific community is becoming increasingly aware of the necessity to model the Earth at finer spatial and temporal resolutions, which also requires better descriptions of the chemical, physical and biological processes involved. The standard formulations for the gas transfer velocities and solubilities are 24 and 36 years old, respectively, and recently, new alternatives have emerged. We developed a framework congregating the geophysical processes involved which are customizable with alternative formulations with different degrees of complexity and/or different theoretical backgrounds. We propose this framework as basis for novel couplers of atmospheric and oceanographic model components. We tested it with fine resolution data from the European coastal ocean. Although the benchmark and alternative solubility formulations agreed well, their minor divergences yielded differences of many tons of greenhouse gases dissolved at the ocean surface. The transfer velocities largely mismatched their estimates, a consequence of the benchmark formulation not considering factors that were proved determinant at the coastal ocean. Climate Change research requires more comprehensive simulations of atmosphere-ocean interactions but the formulations able to do it require further calibration and validation.

Keywords: solubility, transfer velocity, Henry constant.

1 Introduction

Earth-System as well as Regional models are ensembles of inter-connected components, namely the land, ocean, atmosphere and cryosphere. The exchange of information between each pair requires specific couplers that are also responsible for the estimation of geophysical processes specific to their physical interfaces. In this work we focus on the coupling between the atmospheric and the oceanographic components, and on the estimation of the air-water fluxes of greenhouse gases. In order to test and compare different algorithms and degrees of complexity, we developed a framework allowing to set specific customizations. Furthermore, this framework is able to automatically select simpler algorithms in particular locations where the lack of data does not allow using more comprehensive formulations. The framework can be applied to estimate the air-water fluxes of any gas on the atmosphere, including DMS, by selecting the respective constants. The solubility constants are provided by Sarmiento and Gruber (2013) or Sander (2015). The Code and Data Availability section has the link to the software, data and videos.

Because the oceans can act as sinks or sources of greenhouse gases and dimethyl sulfide (DMS) to the atmosphere, the dynamics of their gas exchanges are fundamental for Earth's climate. The open ocean is generally believed to uptake CO_2 from the atmosphere, despite the observed seasonal, inter-annual and regional variability. In the sub-polar regions the solubility pump retrieves large amounts of greenhouse gases from the atmosphere and transports them to the deep ocean. On the other hand, the balances and fluxes of CO_2, CH_4, N_2O and DMS at the coastal oceans' surface are very heterogenic due to factors like upwelling, plankton productivity and continental loads. Earth-System Models (ESM) and marine biogeochemistry have difficulties simulating these processes na their inherent variability. Constrained by computational demands, they usually simulate the biosphere at decadal and centennial time-scales with daily intervals and spatial resolutions of hundreds to one thousand kilometres. Such are the cases of ESM applications by the Intergovernmental Panel on Climate Change (IPCC), Max Planck Institute (MPI) or Centro Euro-Mediterraneo sui Cambiamenti Climatici (CMCC). Hand-in-hand with the low resolution for space and time, they estimate the atmosphere-ocean gas fluxes from simpler formulations that disregard the complexity of processes more recently unveiled at the coastal ocean. The generalization by Wanninkhof (1992), relying on wind speed (u_{10}) as the sole driver of transfer velocity, is the standard in current ESM at coarse resolutions. The regional oceanographic numerical lab MOHID allows the user to choose between the air-water gas exchange formulations proposed by Carini et al. (1996) or Raymond and Cole (2001), only accounting for u_{10}, or by Borges et al. (2004), also accounting for current drag with the bottom. These are empirical formulations best fitting low wind data collected from estuaries. There are many other simpler formulations estimating the air-water gas exchange considering a few factors that were determinant for that specific set of environmental conditions and optimizing the adjustment to the data used in their calibration (see the list of available formulations in the software settings). However, modelling the coastal oceans with fine resolution requires an algorithm that, whatever the local conditions, is always able to forecast with improved accuracy due to its enhanced representation of the multitude of processes potentially present. Developing such algorithm demands for a framework able to be updated with the best formulation for each of the mediator processes involved.

The Flux of Gases (FuGas) version 2.2 is an upgrade of the framework by Vieira et al. (2013) congregating several of the geophysical processes involved in the air-water gas exchanges, and where each process can be simulated by one formulation chosen from an extensive list. It includes 52 alternative formulations to account for such factors as solubility, wind or current mediated turbulence, atmospheric stability, sea-surface roughness, breaking waves, air and water viscosities, temperature and salinity. We use this framework to compare between the estimations of the solubilities and fluxes of greenhouse gases using the ESM standards and recent alternative formulations. First, we tested with field data from the Baltic Sea. Then, we coupled the Weather Research and Forecasting (WRF) atmospheric model to the WaveWatch III (WW3) - NEMO oceanographic model using simulated data from the European coastal ocean. The calculations were vectorized and parallelized for improved computational speed.

2 Methods

Air-water gas fluxes result from the interaction of two factors: (i) the unbalance between the gas concentrations in the air and in the water sets the strength and direction of the flux, and (ii) the resistance the medium does for being crossed by the flow. The traditional formulation estimates the flux from $F=k_w \cdot k_H cp \cdot \Delta p_{gas}$, in units of $mol \cdot m^{-2} \cdot s^{-1}$. The $k_H cp$ is the Henry's constant for the gas solubility in its C_w/p_a form ($mol \cdot m^{-3} \cdot atm^{-1}$), where p_a is its air partial pressure (atm) and C_w its concentration in the water ($mol \cdot m^{-3}$). Sander (2016) provided the $k_H cp$ in units of $mol \cdot L^{-1} \cdot atm^{-1}$, and thus conversion was required. The Δp_{gas} is the difference between air and water gas partial pressures (atm) i.e, pX_a-pX_w. In this form a positive flux represents uptake by the ocean. The pX_a must be corrected for the partial pressure of water vapour considering saturation over the sea-surface: $pX_{moist}=(1-p_{H2O}/P)p_{dry}$. This conversion is detailed in section (2.1) below. The k_w is the transfer velocity of gases across the sub-millimetrically thick water surface layer in $m \cdot s^{-1}$ although usually plotted in $cm \cdot h^{-1}$. For mildly soluble gases the airside resistance is not negligible. In these cases, the double layer model (Liss and Slater, 1974) estimates the flux taking into consideration both the water-side and air-side sub-millimetrically thick surface layers and thus, $F = K_w(C_a/k_H-C_w) = K_a(C_a-C_w \cdot k_H)$. The C_a and C_w are the concentrations of the gas in air and water given in $mol \cdot m^{-3}$ and the k_H is Henry's constant in its equivalent dimensionless quantity (C_a/C_w). The transfer velocity is estimated from both layers as $K_w=(1/k_w+1/(k_H \cdot k_a))^{-1}$ or its equivalent $K_a=(k_H/k_w+1/k_a)^{-1}$.

2.1 Solubility

Sarmiento and Gruber (2013) compiled the algorithm for the $k_H cp$ dependence on temperature and salinity provided by Weiss (1974) and Weiss and Price (1980). We converted it to its corresponding dimensionless k_H preserving the constants required to estimate Bunsen's solubility coefficient β. This formulation accounted for fugacity (f) of non-ideal gases (Eq. 1) and corrected the gas partial pressure for moisture effects from the expression $p_{moist}=(1-p_{H2O}/P)p_{dry}$ considering water vapour saturation over the sea-surface (Eq. 2). P is air pressure (atm), T_w is water temperature (K), S is salinity (‰), p is the gas partial pressure (atm), R is the ideal gas law constant ($Pa \cdot m^3 \cdot mol^{-1} \cdot K^{-1}$), V_m is the molar volume of the specific gas (22.3 for CO_2 and CH_4, and 22.2432 for N_2O) and V_{ideal}=22.4136 $mol \cdot L^{-1}$ is the molar volume of ideal gases. Solubility coefficients were estimated from the Virial expansion (Eq. 3), where B was β or β/V_m, depending on which gas it was applied to (Table 3.2.2 in Sarmiento and Gruber (2013)). Our software automatically detected the gas from the a_i coefficient. When B=β the k_H was estimated from Eq. (4). When $B=\beta/V_m$ the k_H was estimated from Eq. (5).

$$f = \exp\left(\frac{101.325P(V_m - V_{\mathrm{ideal}})}{\mathrm{RT}_w}\right) \quad (1)$$

$$\log\frac{p_{H_2O}}{P} = 24.4543 - 67.4509\left(\frac{100}{T_w}\right) - 4.8489\ln\left(\frac{T_w}{100}\right) - 0.000544S \quad (2)$$

$$\log(B) = a_1 + a_2\frac{100}{T_w} + a_3\log\frac{T_w}{100} + a_4\left(\frac{T_w}{100}\right)^2 \\ +S\cdot\left(b_1 + b_2\frac{T_w}{100} + b_3\left(\frac{T_w}{100}\right)^2\right) \tag{3}$$

$$k_H = \left(1 - \frac{p_{H_2O}}{P}\right)\frac{101.325V_m}{\mathrm{RT}_w\beta f} \tag{4}$$

$$k_H = \frac{101.325}{\mathrm{RT}_w\beta f} \tag{5}$$

Johnson (2010) developed an algorithm from an alternative chemistry background. It accounts for the effects of temperature and salinity taking into consideration the molecular and thermodynamic properties of the water, its solutes and the specified gas, but disregarding the non-ideal behaviour of the gases and moisture. His formulation was developed from the compilation by Sander (2015) (although available in the web since 1999) of the $k_H cp$ for nearly all gases in the atmosphere at 25º C (298.15 K) and 0 ppt. Then, equation (6) converted the $k_H cp$ to k_H at a given temperature and 0 ppt salinity. The term $-\Delta_{soln}H/R$ reflected the temperature (in Kelvin) dependence of solubility, having a value of 2400 for CO_2, 1700 for CH_4 and 2600 for N_2O. The correction to a given salinity (Eq. 7) relied on the empirical Setschenow constants ($K_S=\theta\cdot\log Vb$) reporting the effect of electrolytes salting-out gases proportionally to their liquid molar volume at boiling point (Vb). The Vb was estimated using the additive Schroeder method, whereas θ was estimated from Eq.8 using a provisional $k_{H\#}=0.0409/k_H cp$.

$$\mathrm{k}_{\mathrm{H},0} = \frac{12.1866}{P\cdot T_w\cdot k_{H,cp}\cdot e^{\frac{-\Delta_{\mathrm{Soln}}H}{R}(1/T_w - 1/298.15)}} \tag{6}$$

$$k_H = k_{H,0}\cdot 10^{K_s S} \tag{7}$$

$$\theta = 7.33532\cdot 10^{-4} + 3.39615*10^{-5}\cdot\log(k_{\mathrm{H\#}}) \\ -2.40888\cdot 10^{-6}\cdot\log(k_{\mathrm{H\#}})^2 \\ +1.57114\cdot 10^{-7}\cdot\log(k_{\mathrm{H\#}})^3 \tag{8}$$

The mismatches between both algorithms lead to differences in the estimates of greenhouse gases dissolved in the first meter below the ocean surface, which were calculated from $\Delta ton\cdot m^{-1}\cdot 121\ km^{-2} = 11^2\cdot\Delta s\cdot p_{gas}\cdot P\cdot 101325\cdot M_a/(10^9\cdot R\cdot T)$. The Δs was the difference in the solubilities estimated by both algorithms and converted to the C_w/C_a form. Hence, $\Delta s=1/k_{H'Sar13'}-1/k_{H'Joh10'}$, and because C_a was equal among them, the $\Delta s= (C_{w'Joh10'}-C_{w'Sar13'})/C_a$. This difference of $mol\cdot m^{-3}$ of gas in the water per $mol\cdot m^{-3}$ of gas in the air at each cell was averaged over the 66 h time interval. In order to convert from mols to grams in the water we multiplied by the molar mass of the specific gas (M_g), which is 44.01 for CO_2, 16.043 for CH_4 and 44.013 for N_2O. Then, we divided by 10^6 to convert from grams to tons. We still needed to estimate C_a from the atmospheric pressure (P) and the partial pressure (p_{gas}) of CO_2, CH_4 or N_2O, 390 ppm, 1.75 ppm and 0.325 ppm respectively (EPA, 2015), assuming that they were approximately uniform all over the atmospheric surface boundary layer (SBL). Using the ideal gas law, we divided by R and T (in Kelvin), multiplied by 101325 to convert Pascal to atm and divided by 10^6 to re-scale from ppm to unity. Finally, we multiplied by $(11\ km)^2$ to have the total difference in mass dissolved in the first meter below the surface of 11 km wide cells.

2.2 Transfer velocity

The available algorithms consider that the rate at which gases cross the sea-surface is basically set by the turbulence upon it. E.g. wind drag, wave breaking, currents and rain promote turbulence. The water viscosity, set by temperature and salinity and enhanced by the presence of surfactants, antagonizes turbulence. Figure 1 in the work by Wanninkhof et al. (2009) clarifies how some of these processes interact. With all these forcings, it becomes difficult to develop an algorithm that estimates the transfer velocity accurately. The literature has many of them, either fitted to specific surface conditions or rougher generalizations, focusing on different factors and relying in different theoretical backgrounds. The simpler ones rely on the wind velocity 10m above the sea-surface (u_{10}). Among then, the formulation by Wanninkhof (1992) (henceforth also mentioned as 'Wan92') became the standard used in ESM and satellite data processing (equation 9a,b). It further considers the Schmidt number of the water (Sc_w) related to viscosity and with its exponent reflecting the surface layer's rate of turbulent renewal. Under low winds, the transfer velocity of CO_2 is chemically enhanced due to reaction with water (α_{Ch}) and scales with temperature.

$$k_w = (\alpha_{\mathrm{Ch}} + 0.31 \cdot u_{10}^2)\left(\frac{\mathrm{Sc}_w}{660}\right)^{-0.5} \tag{9a}$$

$$\alpha_{\mathrm{Ch}} = 2.5 \cdot (0.5246 + 0.0162 T_w + 0.000499 T_w^2) \tag{9b}$$

Other simple empirical formulations based only on u_{10} (Carini et al., 1996; Raymond and Cole, 2001), or also accounting for current drag with the bottom (Borges et al., 2004), used data collected in estuaries under low wind conditions. However, modelling the coastal ocean at finer resolutions requires an enhanced representation of the multitude of processes involved. Hence, we updated the framework by Vieira et al. (2013), with the k_w being decomposed into its shear produced turbulence (k_{wind}) and bubbles from whitecapping (k_{bublle}) forcings (Asher and Farley, 1995; Borges et al, 2004; Woolf, 2005; Zhang et al., 2006). Sc_w was determined from temperature and salinity following Johnson (2010):

$$k_w = (\alpha_{\mathrm{Ch}} + k_{\mathrm{bubble}} + k_{\mathrm{wind}} + \mathrm{k}_{\mathrm{current}}) \cdot (600/\mathrm{Sc}_w)^{0.5} \tag{10}$$

The formulation by Zhao et al. (2003), merged k_{wind} into k_{bubble} (Eq. 11a) using the wave breaking parameter (R_B given by Eq. 11b). The u_* is the friction velocity i.e, the velocity of wind dragging on the sea-surface, and f_p is the peak angular frequency of the wind-waves. The kinematic viscosity of air (υ_a) was estimated from Johnson (2010). This solution used the wave field as a proxy for whitecapping that increased transfer velocity with wind-wave age. However, it simultaneously used the wave field as a proxy for the sea-surface roughness that increased transfer velocity from wind-drag over steeper younger waves (through the WLLP estimation of u_* explained in a section below).

$$k_{\mathrm{bubble}} = 0.1315 \cdot R_B^{0.6322} \tag{11a}$$

$$R_B = \frac{u_*^2}{2\pi f_p \nu_a} \tag{11b}$$

A more comprehensive solution split the two drives of transfer velocity (Woolf, 2005; Zhang et al., 2006): k_{wind} for the transfer mediated by the turbulence generated by wind drag (Eq. 12, taken from Jähne et al., 1987) and k_{bubble} for the transfer mediated by the bubbles generated by breaking waves (Eq. 13). B is Bunsen's solubility coefficient estimated for the local sea-surface conditions. $W=3.88\times10^{-7}R_B^{1.09}$ is the whitecap cover requiring the R_B estimated from Eq. (11b), V=4900, e=14 and n=1.2.

$$k_{\mathrm{wind}} = 1.57 \cdot 10^{-4} \cdot u_* \tag{12}$$

$$k_{\mathrm{bubble}} = \frac{\mathrm{WV}}{B}\left[1 + \left(e \cdot B \cdot \mathrm{Sc}_{w^{-1/2}}\right)^{-1/n}\right]^{-n} \tag{13}$$

These formulations required friction velocity (u_*), which was estimated from the Wind Log-Linear Profile (WLLP: Eq. 14) accounting for wind speed at height z (u_z), atmospheric stability of the surface boundary layer (through ψ_m) and sea-surface roughness (through the roughness length z_0). The κ is von Kármàn's constant. Historically, the WLLP originated from the Monin-Obukhov Similarity Theory (Monin and Obukhov, 1954; Stull, 1988).

$$u_* = \frac{u_z \cdot \kappa}{\ln(z) - \ln(z_0) + \psi_m(z, z_0, L)} \tag{14}$$

Roughness length (z_0) is the theoretical minimal height (most often sub-millimetrical) at which wind speed averages zero. It is dependent on surface roughness and often used as its index. It is more difficult to determine over water than over land as there is a strong bidirectional interaction between wind and sea-surface roughness. Taylor and Yelland (2001) proposed a dimensionless z_0 dependency from the wave field, increasing with the wave slope (Eq. 15). Here, H_s is the significant wave height and L_p is the peak wave period. Due to the bidirectional nature of the z_0 and u_* relation, we also tested an iterative solution (iWLP) where Eq.15 was used as a first guess for the z_0 and Eq.14 for its subsequent u_*. A second iteration re-estimated z_0 from the COARE 3.0 (Fairall et al.; 2003) adaptation of the Taylor and Yelland (2001) formulation, which added a term for smooth flow (Eq. 16), and u_* again from Eq.14. Applying four iterations were enough for an excellent convergence of the full data array. Irrespective of the WLLP or iWLP algorithm, the coefficients proposed by Taylor and Yelland (2001) applied to our data sometimes yielded incredibly high and unreal z_0 leading to absurdly high u_* and k_w. To prevent this bias we imposed a maximum roughness length $z_{0,max}$=0.01 m.

$$\frac{z_0}{H_s} = 1200 \cdot \left(\frac{\mathrm{H_s}}{\mathrm{L_p}}\right)^{4.5} \tag{15}$$

$$z_0 = 1200 \cdot H_s \left(\frac{H_s}{L_p}\right)^{4.5} + \frac{0.11\nu_a}{u_*} \tag{16}$$

Atmospheric stability characterized the tendency of the surface boundary layer (SBL) to be well mixed (unstable SBL with $\psi_m<0$) or stratified (stable SBL with $\psi_m>0$). The ψ_m was inferred from the 'bulk Richardson number' (Ri_b: Eq. 17), weighting the air vertical heat gradient and kinetic energy, and requiring the air virtual potential temperature (T_v) estimated from air temperature (T in ºC), air pressure (P in atm), humidity (dimensionless) and the gravitational acceleration constant (g). Grachev and Fairall (1997) estimated $T_v=T_p(1+0.61q)$, where T_p is the air potential temperature and q the observed specific humidity . Stull (1988) estimated $T_v=T_p(1+0.61\cdot r_{sat}\cdot h_r+r_L)$, where r_{sat} is the water vapour mixing ratio at saturation, h_r is the observed relative humidity and r_L the observed liquid water mixing ratio. T_p (in ºC) was estimated from $T_p = T_k(1000/(1013.25P))^{0.284}$, where T_k is temperature (Kelvin). The r_{sat} =

$0.622e_{sat}/(101.32501P-e_{sat})$ and the $\ln(e_{sat}) = \ln 0.61078 + 17.2694T/(T_k-35.86)$. Alternatively, Lee (1997) estimated the Ri_b directly from the air potential temperature neglecting humidity. The wind velocity (u_z), temperature (T_z), pressure (P_z) and humidity (q_z) z meters above sea-surface were given by the WRF second level. The wind velocity at z_0 (u_0) was set to the theoretical $u_0=0$. Temperature at the height of 0 m (T_0) was given by the SST (Grachev and Fairall, 1997; Fairal et al., 2003; Brunke et al., 2008) without rectification for cool-skin and warm-layer effects due to the lack of some required variables. Yet, these effects tend to compensate each other (Brunke et al., 2008; Fairall et al., 1996; Zeng and Beljars, 2005). Air pressure at 0 m (P_0) was given by the WRF at the lower first level (at roughly 0 m). Humidity at 0 m (q_0) was set to the saturation level at P_0 and T_0 using $q=r_{sat}/(1+r_{sat})$ (Grachev and Fairall, 1997). The Ri_b was used to estimate the length L from the Monin-Obukhov's similarity theory, a discontinuous exponential function tending to $\pm\infty$ when Ri_b tends to ± 0 and tending to ± 0 when Ri_b tends to $\pm\infty$. Ri_b and L were used to estimate ψ_m following Stull (1988) or Lee (1997) algorithms.

$$\mathrm{Ri}_b = \frac{g\Delta T_v \Delta z_i}{T_v \cdot u_z^2} \tag{17}$$

The transfer velocity of mildly soluble gases, besides taking into consideration the molecular crossing of the water-side surface layer, should also take into consideration the molecular crossing of the air-side surface layer (Liss and Slater, 1974, Wanninkhof et al., 2009; Johnson, 2010). We compared between the use of the traditional single layer model and the double layer "thin film" model (Liss and Slater, 1974), the later estimating the air-side transfer velocity (k_a) from the COARE formulation as in Eq. 18 (Jeffrey et al., 2010). CD is the drag coefficient and Sc_a the Schmidt number of air, which were determined for a given temperature and salinity following Johnson (2010).

$$k_a = \frac{u_*}{13.3 \cdot \mathrm{Sc}_a^{1/2} + \mathrm{CD}^{1/2} - 5 + \frac{\log(\mathrm{Sc}_a)}{2\kappa}} \tag{18}$$

2.3 Validation with field data

The field sampling occurred from the 22nd of May 2014 to the 26th of May 2014 using the atmospheric tower at Östergarnsholm in the Baltic Sea (57° 27′ N, 18° 59′ E), the Submersible Autonomous Moored Instrument (SAMI-CO_2) 1 km away and the Directional Waverider (DWR) 3.5 km away, both south-eastward from the tower (see e.g. Högström et al. (2008) and Rutgersson et al. (2008) for detailed description of the sites). The air-water CO_2 fluxes measured by eddy-covariance were smoothed over 30 min bins and corrected according to the Webb-Pearman-Leuning (WPL) method (Webb et al., 1980). We used only the fluxes for which the wind direction set the SAMI-CO_2 and DWR in the footprint of the atmospheric tower (90º < wind direction < 180º). The DWR measured temperatures at 0.5 m depth, taken as representative for the sea-surface. Salinity was obtained from the Asko mooring data provided by the Baltic In-Situ Near-Real-Time Observations available in Copernicus Marine catalogue. We applied this data set to the single processing ensemble of the FuGas 2.2 in order to test which algorithms provide better approximations to reality.

2.4 Retrieving and processing Level 4 data

The atmospheric model was the standard operational application of the WRF by Meteodata.cz , with 9 km and 1 h resolutions. Air temperature 'T' (ºC), pressure 'P' (atm), U and V components of wind velocity ($m \cdot s^{-1}$), water vapour mixing ratio ‘Q’ (scalar) and height ‘h’ (m), where retrieved at the two lowest levels within the SBL. The vertical thickness of the WRF horizontal layers varied with space and time. Over the ocean, the two lowest levels occurred roughly at 0 m and 12 m heights. The WRF output decomposes height, temperature and pressure into their base level plus perturbation values.

Sea-surface temperature (SST) and salinity (S) were estimated by the NEMO modelling system provided in the MyOcean catalogue with 1/12º and 1 day resolutions. The WW3 wave field data for the Mediterranean Sea was supplied by the Istituto Nazionale di Geofisica e Vulcanologia (INGV) using the WW3-NEMO modelling system at 0.0625 º and 1 h resolutions (Clementi, 2013), and for the North Atlantic by Windguru at roughly 0.5º and 3 h resolutions. The variables included significant wave height ‘H_s’ (m) and peak frequency ‘f_p’ (rad·s^{-1}) for wind sea i.e, disregarding swell. A few aspects did not correspond to the ideal data format for atmosphere-ocean coupling, and required further calculations: (i) The peak wave length ‘L_p’ (m) was estimated from the peak frequency assuming the deep-water approximation: $L_p=2\pi g/f_p^2$, where g is the gravitational acceleration constant; (ii) the Windguru data did not provide wind sea component where (and when) the wind was too low. For these missing cases were attributed the lowest H_s and L_p simulated everywhere else; (iii) the Windguru and the INGV data overlapped along the Iberian shores, in which case the INGV was given a 2:1 weight over the Windguru data.

The WRF and WW3-NEMO outputs were retrieved for the European shores from the 24th of May 2014 at 06h to the 27th of May 2014 at 00 h. All variables were interpolated to the same 0.09º grid (roughly 11 km at Europe’s latitudes) and 1 h time steps. This resulted in a data set with 17 variables × 41776 locations × 66 time instances, that occupied over 1Gb ram memory (with another 1Gb taken by the software). To optimize the computations, the calculations were first vectorized and then parallelized using the Single Program Multiple Data (spmd) programming strategy. Hence, in the FuGas 2.1 multiple processing ensemble (supplied in the interactive discussion of this report), the variables were first organized in matrices with locations along the 1st dimension and time along the 2nd. Running the calculations applying matrix algebra to the whole data set, by itself represented an improved speed of several orders of magnitude. Furthermore, the spmd replicated the data, split the replicates into n approximately equal-sized arrays, and distributed their calculation among the n available cpu cores, which represented an extra improvement of computational speed. However, it also bared computational costs:

(i) invoking the parallel processing toolbox was time consuming,
(ii) replicating over 1Gb ram was time consuming,
(iii) when running the calculations with other programs on the background the 4Gb ram memory was soon exhausted. Thereafter, the use of virtual memory in the hard-disk stalled enormously the calculations. To prevent it the following actions were implemented,
(iv) Programs like the antivirus, backup tools, Office, Skype, Dropbox, etc were shut down in the Task Manager,
(v) the spmd were split into several sequential code blocks and in-between the variables no longer necessary were deleted. This spmd fragmentation was time consuming.

In conclusion, there is no perfect solution for parallel computing, and although spmd is the best strategy available for this task, its application needs to be carefully programmed according to the data and hardware characteristics. Optimizing the data management was one fundamental improvement between the 2.1 and the 2.2 versions of the FuGas. The simulations of the European coastal ocean no longer exhausted the ram memory and did not even use more than 70% of it (using above 90% becomes critical). Consequently, the computation time improved from ≈12 min to ≈4 min.

3 Results

The solubility formulations were compared simulating the range of environmental conditions commonly found in nature: T_w ranged from 4ºC to 30ºC at 1ºC intervals while S ranged from 0 ppt to 36 ppt at 1 ppt intervals. The ratio between the solubilities estimated by each formulation (i.e, $k_{H,Joh10}/k_{H,Sar13}$) showed better how much these could diverge (Fig. 1). Afterwards, both formulations were applied to the conditions observed at the European coastal ocean during the experiment. The estimated solubilities were compared from their ratio averaged over the 66 h time interval using the geometric mean (Fig. 1). From the 24^{th} to the 26^{th} May the water temperature at the ocean surface changed significantly and there were large fresh water inputs from the Black Sea and the Baltic Sea (Video 1). The widest divergences were up to 4.5% in the CO_2 solubility estimates associated to cooler waters, 5.8% in the CH_4 solubility estimates associated to both temperature extremes, and 2.1% in the N_2O solubility estimates associated to cooler and less saline waters (Fig. 1).These mismatches lead to large differences in the estimates of greenhouse gases dissolved in the first meter below the ocean surface (Fig. 2). Integrated over space, these differences summed to 1.17×10^5 ton of CO_2, 7374.5 ton of CH_4 and 25.1 ton of N_2O.

During the Baltic Sea sampling at the Östergarnsholm site the observed Δppm varied within 120 and 270, well below the limit for a 25% error in the flux estimates as reported by Blomquist et al. (2014) for our IRGA model, the LI-COR LI-7500. Even so, the k_w estimated from the Eddy-Covariance (E-C) measurements were close matches to the k_w estimated by both generalistic and comprehensive algorithms (Fig.3). The mismatches found in previous versions of this report were consequence of humidity mistakenly input in incorrect units into the E-C matlab script. The mismatches currently seen at lower wind speeds may be due to failure of the E-C measurements under atmospherically stable conditions, a problem well known to affect E-C methods. During the experiment the SBL was generally stable ($0<Ri_b<0.09$ with a couple of exceptions above 0.09) while the sea-surface was little to moderately rough ($z_0<0.49$ mm). These conditions were used as reference to estimate the elasticity of k_w to the environmental variables (Fig. 4). The variables related with the SBL stability, namely the u_{10}, temperature, pressure and humidity, were able to induce larger changes in k_w. However, the SBL stability changed little during this experiment whereas the sea-state change considerably, with a calmer period during which the sea-surface was smoother and a harsher period during which the sea-surface was rougher (Fig.3). Hence, during this experiment the sea-state had a greater impact on the k_w than the atmospheric stability. The k_w dependency on the sea-state is well-known as it is thought that k_w scales with the turbulent kinetic energy dissipation at the sea-surface (ε) and that this is better reflected by the sea-state (Soloviev et al., 2007, Wang et al., 2015). Accordingly, the COARE 3.0 included the wave state in the estimation of the roughness parameters essential for the transfer of mass, heat and momentum (Fairal et al. 2003) while Frew et al. (2004) observed a remarkable correlation between the k_w and small scale waves. Our comprehensive algorithms adjusted to the sea-state splitting the k_w estimates into two distinct groups relative to each period. The k_w estimated for the rougher sea-states scattered along a steeper line placed above the k_w estimated for the smoother sea-states. The k_w estimated from the E-C measurements tended to follow this same pattern (Fig.3), and episodic departure from it may be inherent to E-C natural variability. The generalistic u_{10}-based formulations were unable to perform this adjustment to the local wave state. Their small k_w fluctuations were a sole consequence of changes in water viscosity (as estimated by the Sc_w) driven by changes in water temperature. Furthermore, the Wan92 formulation and our comprehensive formulations adjusted remarkably well under rougher seas, whereas the Cea96 formulation calibrated with data from the Parker river estuary and our comprehensive formulations adjusted remarkably well under lighter winds and/or smoother seas (Fig.3). These fits clearly show an ability of our comprehensive algorithms to adjust to the local conditions that cannot be met by the generalistic u_{10}-based formulations. This is not a minor detail: at u_{10}≈8 m·s^{-1} the k_w estimated from wind dragging over rougher or over smoother sea-surfaces differed ≈31% while at u_{10}<4 m·s^{-1} the u_{10}-based formulations estimated less than 50% of the k_w estimated by our comprehensive algorithms. Furthermore, under the lowest winds the k_w estimated by u_{10}-based formulations tended to zero, with the exception of the formulations by McGillis et al. (2001) and Wanninkhof et al. (2009) as explained below. This is a bias from reality that has been thoroughly debated during the last decades. The COARE algorithm addressed it by adding a gustiness term to stabilize the k_w in effective velocities under lighter winds (Grachev and Fairall, 1996; Fairall et al., 2003). With the same objective, Clayson et al. (1996) replaced the gustiness term by a capillary wave parameterization. Mackay and Yeun (1983), McGillis et al. (2001), Wanninkhof et al. (2009) and Johnson (2010) added a constant to the k_w equation. In our case, due to the iWLP (equations 14 and 16) and the k_w dependence on u_*, under the lowest winds but as long as there are waves, our comprehensive algorithms always provide effective velocities similar to the estimated by the authors mentioned above. Hence, our solution resembles the solution by Clayson et al. (1996). There was yet the interesting detail of how the WLLP and the iWLP diverged under smoother sea-surfaces (*not shown*), supporting the solution suggested in the COARE 3.0 (Fairall et al., 2003) for the iterative estimation of u_* and z_0.

We performed simulations of the European costal oceans to compare between the ESM standard (the Wan92) and our comprehensive alternatives. We show the comparison with the iWLP-W05va. Their k_w estimates diverged mostly under unstable SBL, very rough or very smooth sea-surfaces, or higher friction velocities (Fig. 5). The details of the simulations and the differences between k_w estimates are presented hereafter.

Strong winds occurred along the European shores from the 24th to the 26th of May of 2014. Besides, the air was unusually cold for the season and colder than the sea-surface (Video 1). The rise of the warmer air, heated by the sea-surface, generated turbulent eddies that enhanced mixing within the SBL. These unstable conditions were identified by Ri_b<0, L tending to $^{-}0$ and ψ_m<0 (Video 2). The mixing of the SBL enhanced u_* and k_w everywhere the wind blew lighter. This situation occurred more frequently and intensively nearby land masses and often associated to cooler continental breezes blowing off-shore. Its correct simulation required the estimation of the Ri_b, L and ψ_m from the algorithms by Grachev and Fairall (1997) and Stull (1988) that account for humidity considering saturation at 0 m heights. The Ri_b estimates neglecting humidity, following Lee (1997), yielded biased estimates of the SBL conditions as consequence of biased estimates of the virtual potential temperature. Stull (1988, page 9), Grachev and Fairall (1996) and Fairall et al. (2003) already highlighted the importance of accounting for humidity.

The sea-surface agitation was very heterogenic, particularly at the coastal ocean where it attained both the highest and the lowest estimated roughness lengths (the z_0 in Video 3). There, the steeper waves, consequence of shorter fetches, should extract more momentum from the atmosphere under similar u_{10} conditions (Taylor and Yelland, 2001; Fairall et al, 2003). Thus, the rougher coastal ocean surfaces were expected to possess more turbulent layers through which gases were transferred at higher rates. The comprehensive formulations simulated this by increasing u_* (and consequently k_{wind}) with z_0 under similar u_z i.e, similar winds generate more drag when blowing over harsher sea-surfaces. Aside the rougher weather, whenever lighter wind blew over smoother sea-surfaces, the iWLP estimated much higher z_0 than the WLLP (video 4), demonstrating that the smooth flow was a fundamental driver for the z_0 under calmer weather. This increase in z_0 lead to significantly higher u_*, often 1.5 times higher and sometimes more, anticipating a significant impact on the k_{wind} estimates.

In some rare situations the algorithms estimated unreasonably high k_w despite the z_0 bounds imposed in the software. To avoid this bias, all k_w estimates were imposed a 200 cm·h^{-1}ceiling. The W05va and the Wan92 formulations often diverged their k_w estimates, particularly in the coastal ocean, both on the Atlantic side and on the Mediterranean side, and mostly associated to storms (Video 5). Integrated over space and time, the Wan92 transferred 33061 km^3 of CO_2 across the ≈5,054,896 km^2 of ocean surface during the 66 h that the experiment lasted, corresponding to 90.8% of the 36392 km^3 of CO_2 transferred by the W05va formulation. However, as the bias occurred in both directions the absolute bias summed to 11880 km^3. These differences were higher at the coastal ocean (Fig. 6), a consequence of the factors that were not taken into consideration by the Wan92 (the ESM standard). Apart the CO_2, the W05va transferred 35479 Km^3 of CH_4 and of N_2O. This formulation was also used to compare between the k_{wind} and k_{bubble} components of k_w. The results showed that the k_{bubble} term was always lower than the k_{wind} term and only close to it in two situations: (i) often in the fetch-unlimited Atlantic, and (ii) in a few storms inside the Atlantic where, given their high winds, fetch was not a limitation. Whatever the greenhouse gas, the differences were negligible between estimating k_w using the single layer or the double layer schemes (Video 5). Nevertheless, it is worth noting that it was again under the Mediterranean storms that the bigger differences were found.

4 Discussion

Both solubility formulations generally estimated similar solubilities despite their distinct chemistry backgrounds. Nevertheless, they did diverge in as much as 0.045 mol·mol^{-1} of CO_2, 0.0015 mol·mol^{-1} of CH_4 and 0.012 mol·mol^{-1} of N_2O (i.e, mol of gas in the ocean surface per mol of gas in the atmosphere) in some of the most sensitive situations for Earth-System modelling and satellite data processing: (i) the cooler marine waters occur closer to the poles, where the solubility pump traps greenhouse gases and carries them to the deep ocean (Sarmiento and Gruber, 2013), and (ii) the warmer and the less saline waters occurring at the coastal ocean and seas, which have regularly been observed having greenhouse gases and DMS dissolved in concentrations highly unbalanced with those of the atmosphere (Nevison et al., 2004; Borges et al, 2005; Barnes and Upstill-Goddard, 2011; Sarmiento and Gruber, 2013; Dutta et al., 2015; Gypens and Borges, 2015; Harley et al., 2015). Therefore, the biases in the estimated total amount of greenhouse gases in the first meter depth of the European coastal ocean during late May 2014 may be an indicator of higher global biases.
The accurate estimation of the transfer velocities of greenhouse gases and DMS across the ocean surface is a fundamental issue for biogeosciences and Earth-System modelling. Previous estimates of CO_2 uptake by the global oceans done by coarse resolution implementations diverged in about 70 % depending on the formulations being used (Takahashi et al., 2002), whereas the wide uncertainty in the ocean N_2O source to the atmosphere mostly originated from the uncertainty in the air–water transfer velocities (Nevison et al., 1995). Despite its importance, the knowledge on this subject is still limited, with plenty of room for improvement. The simpler formulations assume either quadratic or cubic dependencies of k_w from u_{10} depending mostly on the sensing method, time scale and fetch (Wanninkhof, 1992; Nightingale et al., 2000; McGillis et al., 2001; Ho et al., 2006; Sweeney et al., 2007; Wanninkhof et al., 2009). Meanwhile, there were substantial developments on the effects of other factors as wave state, atmospheric stability, currents, surfactants, rain and ice cover. Our framework integrates these factors and allows comparison among algorithms of different degrees of complexity. Furthermore, we programmed it to automatically select simpler algorithms when lacking variables indispensible for the application of the more comprehensive ones. Hence, this framework can also be used as basis for atmosphere-ocean couplers in regional and Earth-system models. Our

comparisons demonstrated that the more comprehensive algorithms outrival the simpler ones by taking into consideration factors that are fundamental for the transfer velocity of greenhouse gases and DMS across the coastal oceans' surface. The most determinant factors were the atmospheric stability of the SBL and the sea-surface roughness. Similar conclusions were recently achieved by Jackson et al. (2012) and Shuiqing and Dongliang (2016).

The more comprehensive formulations still need improvement and validation. It is imperative to calibrate and validate the estimation of transfer velocity (k_w) from friction velocity (u_*) and wind-wave breaking (k_{bubble}), and the roughness length (z_0) from the wave field. All the available formulations for these specific purposes lack robust parameter estimations. Generally, there seems to be a great dependency of the available algorithms from the particular data sets that were used to calibrate them. Nevertheless, there is a general consensus that the k_{bubble} term is fundamental under high wind speeds, with its estimate being central to current k_w research. The latest developments have been on the dependency of k_{bubble} from the interactions among the wind, the wave state, the bubble plume and the properties of the gas being transferred (Woolf et al. 2007; Callaghan et al., 2008, 2014; Goddijn-Murphy et al., 2011, Crosswell, 2015). The effect of sea-spray recently became a prominent topic with the emergence of algorithms like the ones by Zhao et al. (2006) and Wu et al. (2015), and a dedicated section in the latest atmosphere-ocean interactions workshop in Brest. So far, these focused on the momentum transfer from wind to the ocean surface and the attenuation of the friction velocity. It should be interesting to understand how the intrusion of the sea-spray on the atmosphere affects the transfer velocity of gases, being anticipated a process symmetrical to that of the intrusion of bubbles on the ocean. The new algorithms for the effects of surfactants are particularly concerned with the variability of the coastal ocean (Pereira et al., 2016). These no longer associate the surfactants to the Schmidt number's exponent but rather to a coefficient setting a proportional decay of k_w. The effect of sea-ice must take into consideration its distortion of the ocean surface and its effect upon the SBL stability (Loose et al., 2014). Our coupling solution still needs to integrate the effects of the sea-surface cool-skin and warm-layer, surfactants, rain, sea-spray and sea-ice. From these, the cool-skin and warm-layer algorithms are the only with robust calibrations and validations, mostly done under the COARE (Fairall et al., 1996; Fairal et al., 2003; Zeng and Beljars, 2005; Brunke et al., 2008). The addition of complexity to any coupling solution must be carefully thought as these cannot become intricate to the point of computation becoming unbearable for ESM application. Algorithms making extensive use of for-loops are unviable: (i) loops are computationally slow and (ii) can easily become conflictive with vectorization and its coordination with parallel processing. Hence, our software needed a deep restructuration from its original version presented in Vieira et al. (2013). Once done, vectorization *per se* enabled improving calculations roughly 12× faster in a single core.

The COARE algorithm is the state-of-the-art in the estimation of atmosphere-open ocean fluxes. During most of its development it focused on the estimation of the heat and humidity fluxes using a framework with an intricate mathematical structure going deep into the simulation of the geophysical process. Only later did it explicitly address the gas fluxes (Fairall et al, 2003; Blomquist et al., 2006, 2014; Jeffrey et al., 2010). Unfortunately, its complexity is deterrent of application to already computationally intensive geoscientific models. The transferred quantities of heat, moisture and momentum, their transfer coefficients, the dimensionless roughness lengths and the gustiness term are interdependent and must be solved iteratively. The COARE estimation of the ψ_m alone is computationally heavier than the most comprehensive ensemble possible in the FuGas 2.2. The COARE was recently introduced as optional in the MOHID model and software. Our preliminary trials testing the heat transfer took ≈14% longer to run each simulation.

5 Code and Data Availability

Software and data related to this article provided as supplementary material. Software, data and videos related to this article available at http://www.maretec.org/en/models/fugas

6 Acknowledgments:

To windguru.cz for the support providing the wave data.Work funded by ERDF Funds of the Competitiveness Factors Operational Programme - COMPETE and by national funds from the FCT - Foundation for Science and Technology project UID/EEA/50009/2013.

7 References

Asher, W. E. and Farley, P. J.: Phase-Doppler anemometer measurement of bubble concentrations in laboratory-simulated breaking waves, J. Geophys. Res., 100C: 7045-7056, 1995.

Barnes, J. and Upstill-Goddard, R. C.: N_2O seasonal distributions and air-sea exchange in UK estuaries: implications for the tropospheric N_2O source from European coastal waters. J. Geophys. Res. 116, G01006, 2011.

Blomquist, B. W., Fairall, C. W., Huebert, B. J., Kieber, D. J. and Westby, G. R.: DMS sea-air transfer velocity: Direct measurements by eddy covariance and parameterization based on the NOAA/COARE gas transfer model. Geophys. Res. Lett., 33(7), L07601, doi:10.1029/2006GL025735, 2006.

Blomquist, B. W., Huebert, B. J., Fairall, C. W., Bariteau, L., Edson, J. B., Hare, J. E. and McGillis, W. R.: Advances in Air–Sea CO2 Flux Measurement by Eddy Correlation. Boundary-Layer Meteorology, 152(3):245–276, 2014.

Borges, A. V., Vanderborght, J. P., Schiettecatte, L. S., Gazeau, F., Ferron-Smith, S., Delille, B. and Frankignoulle, M.:Variability of the Gas Transfer Velocity of CO_2 in a Macrotidal Estuary (the Scheldt), Estuaries, 27, 593–603, 2004.

Borges, A.V., Delille, B., and Frankignoulle, M.. Budgeting sinks and sources of CO_2 in the coastal ocean: Diversity of ecosystems counts, Geophys. Res. Lett., 32, L14601, doi:10.1029/2005GL023053, 2005.

Brunke, M. A, Zeng, X., Misra, V. and Beljaars, A.: Integration of a prognostic sea surface skin temperature scheme into weather and climate models. J. Geophys Res., 113, D21117, doi: 10.1029/2008JD010607, 2008.

Callaghan, A. H., Deane, G. B. and Stokes, M. D.: Observed physical and environmental causes of scatter in whitecap coverage values in a fetch-limited coastal zone. J. Geophys. Res., 113(C5), 10.1029/2007JC004453, 2008.

Callaghan, A. H., Stokes, M. D. and Deane, G. B.: The effect of water temperature on air entrainment, bubble plumes, and surface foam in a laboratory breaking-wave analog. J. Geophys. Res., 119(11),7463-7482, 2014.

Carini, S., Weston, N., Hopkinson, C., Tucker, J., Giblin, A., and Vallino, J.: Gas exchange rates in the Parker River estuary, Massachusetts. Biol. Bull., 191, 333–334, 1996.

Clayson, C. A., Fairall, ., C. W. and Curry, J. A.: Evaluation of turbulent fluxes at the ocean surface using surface renewal theory. J. Geophys. Res., 101, 28503–28513, 1996.

Clementi E., Oddo P., Korres G., Drudi M. and Pinardi N.: Coupled wave-ocean modelling system in the Mediterranean Sea. Extended abstract to the 13th Int. Workshop on Wave Hindcasting, Banff, Canada, 2013.

Crosswell, J. R.: Bubble clouds in coastal waters and their role in air-water gas exchange of CO2. J. Mar. Sci. Eng., 3, 866-890; doi:10.3390/jmse3030866, 2015.

Dutta, M. K., Mukherjee, R., Jana, T. K. and Mukhopadhyay, S. K.: Biogeochemical dynamics of exogenous methane in an estuary associated to a mangrove biosphere; The Sundarbans, NE coast of India. Mar. Chem., 170, 1-10, 2015.

EPA United States Environmental Protection Agency - Climate Change Indicators in the United States - Atmospheric concentrations of greenhouse gases, http://www.epa.gov/climatechange/science/indicators/ghg/ghg-concentrations.html, last accessed: 27 August 2015.

Fairall, C.W., Bradley, E. F., Godfrey, J. S., Wick G. A., Edson, J. B. and Young G. S.: Cool-skin and warm-layer effects on sea surface temperature, J. Geophys. Res., 101, 1295–1308, 1996.

Fairall, C. W., Bradley, E.F., Hare, J.E., Grachev, A.A., and Edson, J.B.: Bulk parameterization of air-sea fluxes: updates and verification for the COARE algorithm, J. Climate, 16, 571–591, 2003.

Goddijn-Murphy, L., Woolf, D. K. and Callaghan, A. H.: Parameterizations and Algorithms for Oceanic Whitecap Coverage. Journal of Physical Oceanography, 41, 742-756, 2011.

Grachev, A. A. and Fairall, C. W.: Dependence of the Monin–Obukhov Stability Parameter on the Bulk Richardson Number over the Ocean. J. Appl. Meteorol., 36, 406–414, 1997.

Gypens, N. and Borges, A. V.: Increase in dimethylsulfide (DMS) emissions due to eutrophication of coastal waters offsets their reduction due to ocean acidification, Front. Mar. Sci., 1,4. doi: 10.3389/fmars.2014.00004, 2015.

Harley, J. F., Carvalho, L., Dudley, B., Heal, K. V., Rees, R. M. and Skiba, U.: Spatial and seasonal fluxes of the greenhouse gases N2O, CO2 and CH4 in a UK macrotidal estuary, Estuar, Coast. Shelf S., 153, 62, 2015.

Ho, D. T., Law, C. S., Smith, M. J., Schlosser, P., Harvey, M. and Hill, P.: Measurements of air-sea gas exchange at high wind speeds in the Southern Ocean: Implications for global parameterizations, Geophys. Res. Lett., 33, L16611, doi:10.1029/2006GL026817, 2006.

Högström, U., Sahlée, E., Drennan, W. M. Kahma, K. K., Smedman, A.-S., Johansson, C., Pettersson, H., Rutgersson, A., Tuomi, L, Zhang, F. and Johansson, M.: To what extent can we believe measurements on a land-based tower to represent upwind open sea conditions? Boreal Environ. Res., 13, 475-502, 2008.

Jackson, D. L., Wick, G. A. and Hare, J. E.: A comparison of satellite-derived carbon dioxide transfer velocities from a physically based model with GasEx cruise observations. J. Geophys. Res. 117, G00F13, doi:10.1029/2011JC007329, 2012.

Jähne, B., Munnich, K. O., Bosinger, R., Dutzi, A., Huber, W. and Libner, P.: On the parameters influencing air-water gas exchange. J.Geophys. Res., 92, 1937–1949, 1987.

Jeffery, C., Robinson, I., and Woolf, D.: Tuning a physically-based model of the air-sea gas transfer velocity, Ocean Modell., 31, 28–35. doi:10.1016/j.ocemod.2009.09.001, 2010.

Johnson, M. T.: A numerical scheme to calculate temperature and salinity dependent air-water transfer velocities for any gas, Ocean Sci., 6, 913–932, 2010.

Lee, H.N.: Improvement of surface flux calculations in the atmospheric surface layer, J. Appl. Meteorol., 36, 1416–1423, 1997.

Liss, P. S. and Slater, P. G.: Flux of gases across the air-sea interface, Nature, 247, 181–184, 1974.

Loose, B., McGillis, W. R., Perovich, D. Zappa, C. J. and Schlosser, P.: A parameter model of gas exchange for the seasonal sea ice zone, Ocean Sci., 10, 17–28, 2014.

McGillis, W. R., Edson, J. B., Ware, J. D., Dacey, J. W. H., Hare, J. E., Fairall, C. W., and Wanninkhof, R.: Carbon dioxide flux techniques performed during GasEx-98, Mar. Chem., 75, 267–280, doi:10.1016/ S0304-4203(01)00042-1, 2001.

Monin, A. S. and Obukhov, A. M.: Basic laws of turbulent mixing in the surface layer of the atmosphere, Translation by McNaughton, K. available at http://mcnaughty.com/keith/papers/Monin_and_Obukhov_1954.pdf (last access: 22 December 2016), 1954.

Nevison, C. D., Weiss, R. F., and Erickson III, D. J.: Global oceanic emissions of nitrous oxide, J. Geophys. Res., 100, 15809–15820, 1995.

Nevison, C. D., Lueker, T. J. and Weiss, R. F.: Quantifying the nitrous oxide source from coastal upwelling, Global Biogeochem. Cy., 18, GB1018, doi:10.1029/2003GB002110, 2004.

Nightingale, P. D., Malin, G., Law, C. S., Watson, A. J., Liss, P. S., Liddicoat, M. I., Boutin, J., and Upstill-Goddard, R. C.: In Situ Evaluation of Air-Sea Gas Exchange Parameterizations Using Novel Conservative and Volatile Tracers, Global Biogeocheml Cy., 14, 373–387, 2000.

OCMIP: Ocean Carbon-Cycle Model Intercomparison Project, available at: http://ocmip5.ipsl. jussieu.fr/OCMIP, last updated: 2004 (last access: 27 August 2015), 2004.

Pereira, R., Scheneider-Zapp, K. and Upstill-Goddard, R.: Surfactant control of gas transfer velocity along an off-shore coastal transect: results from a laboratory gas exchange tank, Biogeosciences Discuss., doi:10.5194/bg-2016-7, 2016.

Raymond, P. A. and Cole, J. J.: Gas exchange in rivers and estuaries: choosing a gas transfer velocity, Estuaries, 24, 312–317, 2001.

Rutgersson, A., Norman, M., Schneider, B., Petterson, H. and Sahlée, E.: The annual cycle of carbon dioxide and parameters influencing the air–sea carbon exchange in the Baltic Proper, J. Mar. Sys., 74: 381-394, 2008.

Sander, R.: Compilation of Henry's law constants (version 4.0) for water as solvent, Atmos. Chem. Phys., 15, 4399-4981, doi:10.5194/acp-15-4399-2015, 2015.

Sarmiento, J. L. and Gruber, N.:. *Ocean Biogeochemical Dynamics*. Princeton University Press, New Jersey, USA. pp73-100, 2013.

Shuiqing, L. and Dongliang, Z.: Gas transfer velocity in the presence of wave breaking. Tellus B, 68, 27034, 2016.

Soloviev, A., Donelan, M., Graber, H., Haus, B. and Schlüssel, P.: An approach to estimation of near-surface turbulence and CO2 transfer velocity from remote sensing data, J. Mar. Sys., 66, 182-194, 2007.

Stull, R. B.: An introduction to Boundary Layer Meteorology, Kluwer Academic Publishers, Dordrecht, pp151-195, 1988.

Sweeney, C., Gloor, E., Jacobson, A. R., Key, R. M., McKinley, G., Sarmiento, J. L. and Wanninkhof, R.: Constraining global air-sea gas exchange for CO2 with recent bomb ^{14}C measurements, Global Biogeochem. Cy., 21, GB2015, doi:10.1029/2006GB002784, 2007.

Takahashi, T., Sutherland, S. C., Sweeney, C., Poisson, A., Metzl, N., Tilbrook, B., Bates, N.,Wanninkhof, R., Feelyf, R. A., Sabine, C., Olafsson, J., and Nojirih, Y.: Global sea–air CO2 flux based on climatological surface ocean pCO_2, and seasonal biological and temperature effects, Deep-Sea Res., 49, 1601–1622, 2002.

Taylor, P. K. and Yelland, M. J.: The dependence of sea surface roughness on the height and steepness of the waves, J. Phys. Oceanogr., 31, 572–590. 2001.

Vieira, V. M. N. C. S., Martins, F., Silva, J. and Santos, R.: Numerical tools to estimate the flux of a gas across the air–water interface and assess the heterogeneity of its forcing functions. Ocean Sci., 9, 355-375, 2013.

Wang, B., Liao, Q., Fillingham, J. and Bootsma, H. A.: On the coefficients of small eddy and surface divergence models for the air-water gas transfer velocity, J. Geophys. Res. Oceans, 120(3), DOI: 10.1002/2014JC010253, 2015.

Wanninkhof, R.:Relationship between wind speed and gas exchange over the ocean, J. Geophys. Res., 97, 7373–7382, 1992.

Wanninkhof, R., Asher, W. E., Ho, D. T., Sweeney, C. S., and McGillis, W. R.: Advances in quantifying air-sea gas exchange and environmental forcing, Ann. Rev. Mar. Sci., 1, 213–244, doi:10.1146/annurev.marine.010908.163742, 2009.

Webb, E. K., Pearman, G. I. and Leuning, R.: Correction of flux measurements for density effects due to heat and water vapour transfer, Quart. J.R. Meteorol. Soc., 106: 85-100, 1980.

Weiss, R. F.: Carbon dioxide in water and seawater: the solubility of a non-ideal gas, Mar. Chem., 2, 203-215, 1974.

Weiss, R. F. and Price B. A.: Nitrous oxide solubility in water and seawater, Mar. Chem., 8, 347-359, 1980.

Woolf, D. K.: Parameterization of gas transfer velocities and sea state-dependent wave breaking,Tellus B, 57, 87 – 94, 2005.

Woolf, D. K., Leifer, I. Nightingale, P.D., Andreae, M.O.: Modelling of bubble-mediated gas transfer: Fundamental principles and a laboratory test, J. Mar. Sys., doi: 10.1016/j.jmarsys.2006.02.011, 2007.

Wu, L., Rutgersson, A. and Sahlée, E.: The impact of waves and sea-spray on modelling storm track and development, Tellus A, 67, 27967, 2015.

Zeng, X. and Beljaars, A.: A prognostic scheme of sea surface skin temperature for modelling and data assimilation. Geophys. Res. Lett., 32, L14605, 2005.

Zhang, W., Perrie, W. and Vagle, S.: Impacts of winter storms on air-sea gas exchange. Geophys. Res. Lett., 33, L14803, 2006.

Zhao, D., Toba, Y., Suzuki, Y., and Komori, S.: Effect of wind waves on air-sea gas exchange: proposal of an overall CO_2 transfer velocity formula as a function of breaking-wave parameter, Tellus B, 55, 478–487, 2003.

Zhao, D., Toba, Y., Sugioka, K. and Komori, S.: New sea spray generation function for spume droplets. J. Geophys. Res., 111(C2), doi: 10.1029/2005JC002960, 2006.

8 Figures

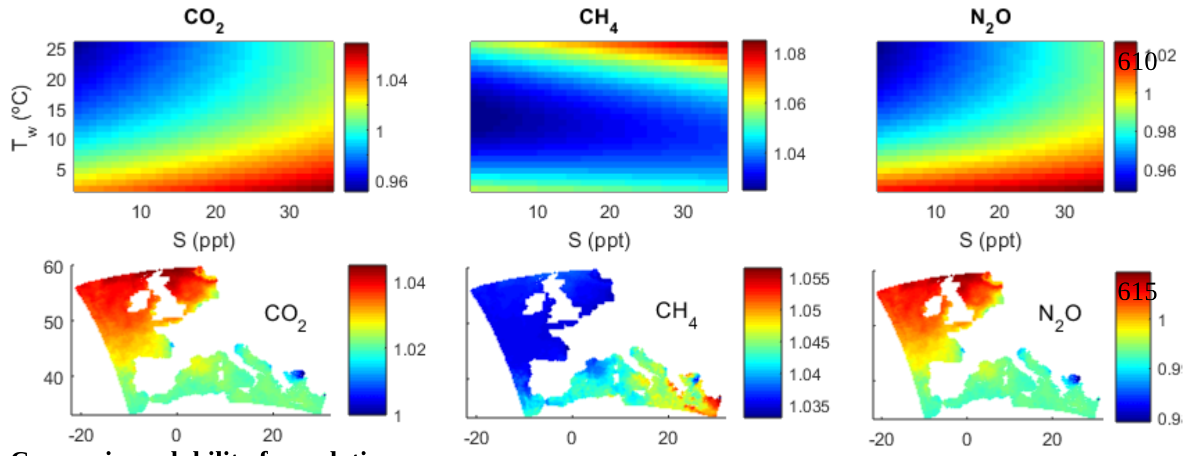

Figure 1: Comparing solubility formulations

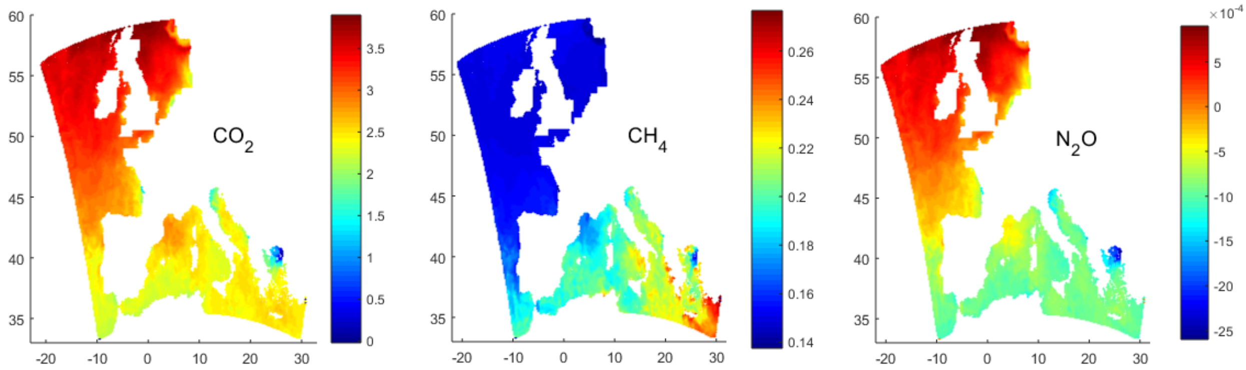

Figure 2: Bias in the gas mass balance for the European coastal ocean

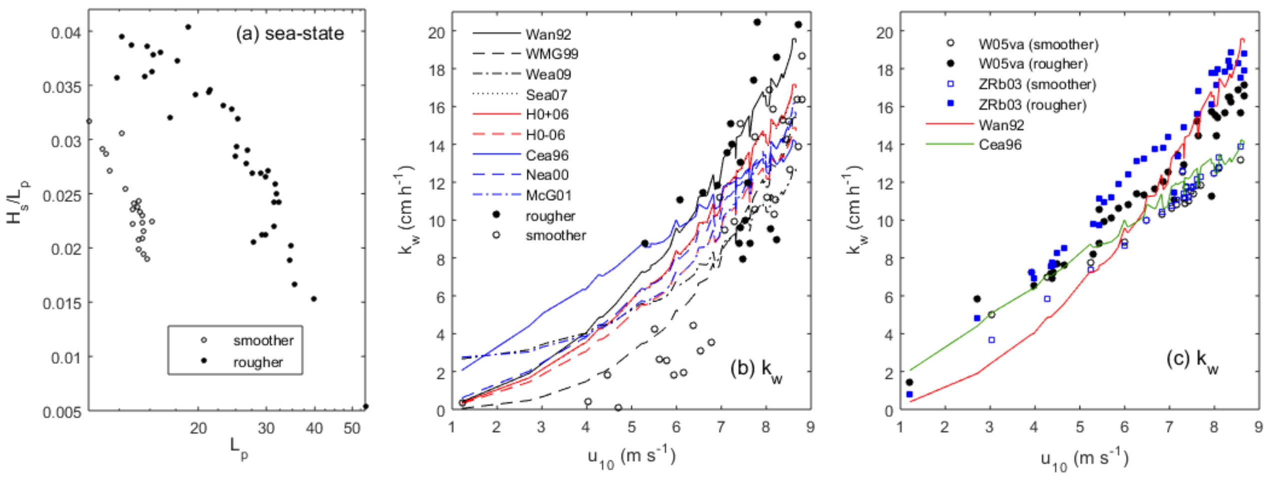

Figure 3: **Comparing transfer velocity algorithms using the data observed at the Baltic.**

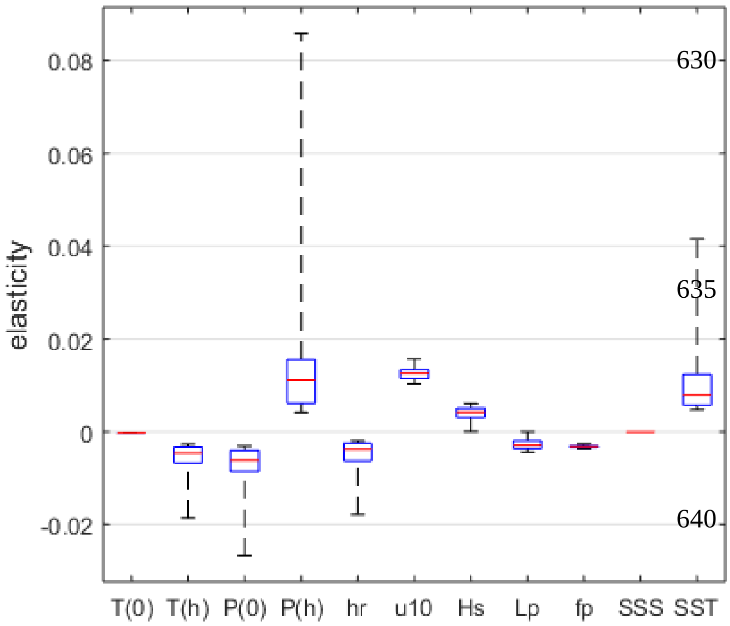

Figure 4: **Elasticities of the transfer velocity to the environmental variables**.

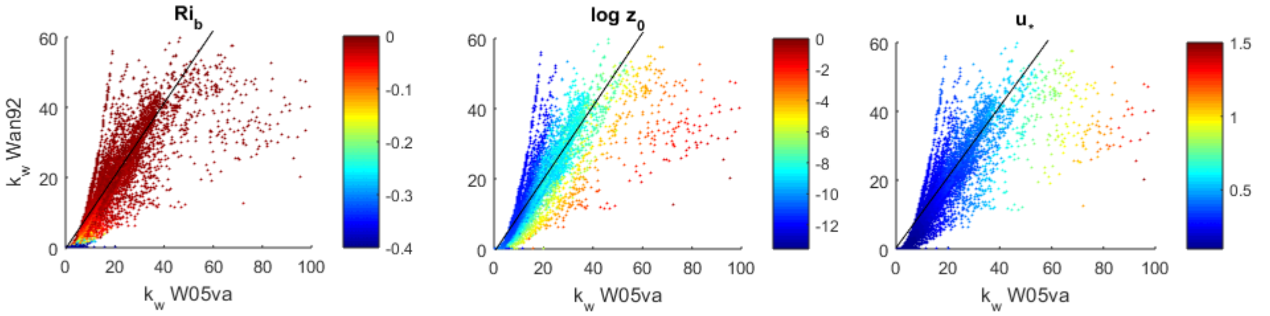

Figure 5: Applying the modelled data about the European coastal ocean for a direct comparison between the k_w estimates.

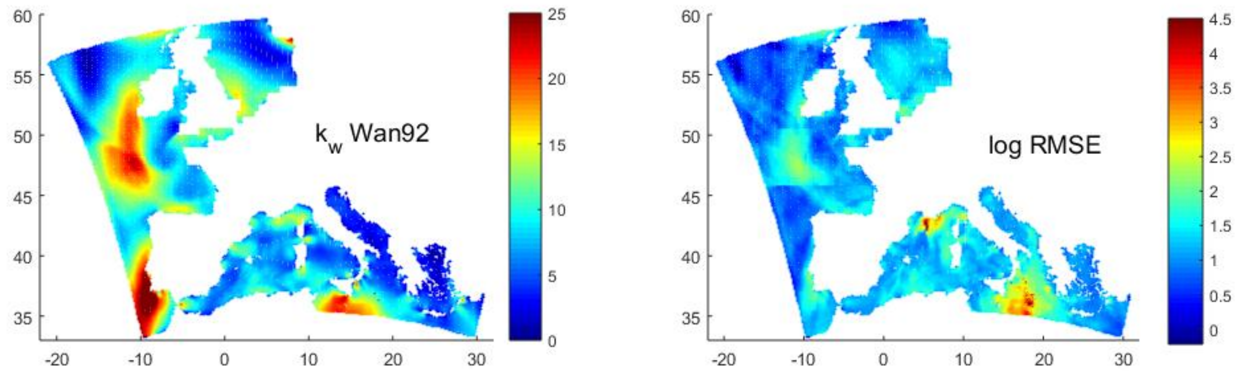

Figure 6: Comparing transfer velocity algorithms using modelled data

9 Figure legends

Figure 1: Comparing solubility formulations: match-mismatch between formulations estimating solubilities of the greenhouse gases CO_2, CH_4 and N_2O according to water temperature (T_w), salinity (S) and location. Colorscale is quotient between k_H estimated from Johnson, 2010 ($k_{H\text{'Joh10'}}$) and k_H estimated from Sarmiento and Gruber, 2013 ($k_{H\ \text{'Sar13'}}$) i.e, $k_{H\text{'Joh10'}}/k_{H\ \text{'Sar13'}}$.

Figure 2: Bias in the gas mass balance for the European coastal ocean: comparing algorithm by Johnson (2010) to compilation by Sarmiento and Gruber (2013). Colorscale: Δton $\cdot m^{-1} \cdot 121\ km^{-2}$ i.e, bias in the gas mass estimated by each algorithm (Δton) for the first meter depth (m^{-1}) in 11 km wide cells ($121\ km^{-2}$).

Figure 3: Comparing transfer velocity algorithms using the data observed at the Baltic. (a) sea-surface roughness given by significant wave height (H_s) and peak wave period (L_p). (b) the k_w estimated by u_{10}-based formulations (lines)and compared to the k_w estimated from the Eddy-Covariance measurements (circles). (c) comparing the k_w estimated by u_{10}-based formulations (lines) and by comprehensive alternatives (circles). Simple formulations by 'Wan92' - Wannninkhof (1992), 'WMG99' – Wanninkhof and McGillis (1999), 'We09' – Wanninkhof et al. (2009), 'Sea07' – Sweeney et al. (2007), 'Nea00' – Nigthingale et al. (2000), 'McG01' – McGillis et al. (2001), 'Ho+06' – upper boundary in Ho et al. (2006) 'Ho-06' – lower boundary in Ho et al. (2006) . Comprehensive formulations were assembled using the 'iWLP' – iteratively estimated wind log-linear profile and included the 'Jea87' – Jähne et al (1987), 'ZRb03' - Zhao et al (2003), and 'W05av' – Woolf (2005) with the kinematic viscosity of air.

Figure 4: Elasticities of the transfer velocity to the environmental variables. Elasticities $(\partial k_w/k_w)/(\partial x/x)$ estimated using the data observed at the Baltic. The k_w was estimated by the iterative wind log-linear profile (iWLP) with the Zhao et al (2003) k_{bubble} term (ZRb03) for the 60 observations in the Baltic. The box-and-wiskers represent the quartiles.

Figure 5: Applying the modelled data about the European coastal ocean for a direct comparison between the k_w estimates by the ESM standard –Wan92 - and a comprehensive formulation - W05va - including the k_{bubble} term by Woolf (2005), the k_{wind} term by Jahne et al. (1987), the z_0 term from the COARE 3.0 and the iterative wind log-linear profile. The z_0 is given in m and the u_* in $m \cdot s^{-1}$.

Figure 6: Comparing transfer velocity algorithms using modelled data: (k_w CO_2 Wan92) transfer velocity of CO_2 estimated from the formulation by Wanninkhof (1992) and averaged over the 66 h; (RMSE) Root Mean Square Error between estimating the transfer velocity using the formulation by Wanninkhof (1992) or the formulation by Woolf (2005) conjugated with the iterative wind log-linear profile.